Chapter 3

Computational Simulation as an Innovative Approach in Personalized Medicine

Bauer Sabine and Paulus Dietrich

Additional information is available at the end of the chapter

http://dx.doi.org/10.5772/intechopen.68835

Abstract

Background: Statistical analyses show that both the spine curvature and the morphological properties of the vertebral bodies can differ considerably. Therefore, the best outcome of a surgery for the individual patient could be achieved by developing patient specific implants to prevent inadequate anchorage of implants that don't optimally fit to the anatomy and can cause damages of spinal structures.

Objective: The aim of our work is to develop patient-specific biomechanical simulation models of the spine to determine the patient-specific load situation and to open up the possibility of developing implant designs that are adapted to the morphological contours of the patients' endplates, which ensures an optimal fit and a balanced load distribution.

Methods: Our approach is the scientific fusion of the fields "medical imaging" and "biomechanical computer modeling." The individual characteristics of patients will be visualized and analyzed through medical imaging. The surface models together with the estimated biomechanical properties can be transferred into biomechanical multibody simulation models.

Results: Taking the patient-specific characteristics and the material properties of the implant into account, simulation models are created to simulate preoperatively the biomechanical effects of new implant designs. In this way, the load situation of the modeled spinal structures can be determined.

Keywords: personalized medicine, computational simulation, medical imaging, surgical planning, patient-specific implants

1. Introduction

Each human has individual physical characteristics and differs not only in his individual anthropometry and morphology but also in the biomechanical properties of his various

biological structures. In order to take these individual factors into account, medicine is going to great lengths to offer tailor-made intervention to individual patients. In the last few years, "individualized medicine" has been addressed as a significant development in medicine. In individualized medicine, products are only suitable for the target patient, but not in a comparable way for others. Overall, individualized medicine can be divided into five different typologies [1]:

1. Biomarker-based stratification
2. Genome-based information about health-related characteristics
3. Determination of risk of disease
4. Differential offers for intervention
5. Therapeutic unique devices.

Therapeutic uniqueness is understood as an individual patient's tailor-made therapeutic device. The idea of individualized devices is not restricted to a specific medical area, but is used in different medical applications. Examples of such individual medical devices are as follows:

- Artificial pancreas device system, as a device under clinical investigation that automatically monitors patient's glucose levels and delivers patient-tailored insulin doses in people with diabetes.
- Software-based quantitative electrocardiogram (EEG) analysis to predict an individual's response to various psychotropic drugs.
- Tinnitus masker, which is personalized by the manufacturer to patient tinnitus.
- Zenith Fenestrated AAA Endovascular Graft as an indicator for the endovascular treatment of patients with abdominal aortic or aortoiliac aneurysms having morphology suitable for endovascular repair [2].

In spinal surgery, it is common practice to use magnetic resonance imaging (MRI) or computed tomography (CT) imaging to assemble, for example, pedicle screw spinal systems consisting of a rod, screw, hook-connector kit to take the patient's individual physiology into account. Currently, the pedicle screw spinal systems are available in different standardized sizes, which fulfill different requirements. In some of these standard implants, for example, there is also the possibility of adjusting the inclination angles of the contact surfaces of the implant to the vertebral body. Despite these adjustment possibilities, due to the very different anatomical conditions of the patents, in some cases only an insufficient anchoring of the implant can be achieved. Further reasons for the need of more precise individualized implants are disease-specific requirements. The aim is to improve the surgical outcome through an exact individual adaptation and adequate fitting to individual anatomical needs [3]. A modern manufacturing process for such therapeutic

uniqueness is a patient-specific production by means of "rapid prototyping," in which the individualization is based on the manufacturing process of the single-unit production [1].

A further step in individualized manufacturing process could be the integration of a preoperative simulation of the spinal stress situation taking the biomechanical conditions of the respective patient into account. This will allow a prediction of the effects of the surgical procedure and an identification of the best possible surgical option. How this would be implemented in a clinical workflow practice is discussed in the subsequent section by means of an extended process chain of rapid prototyping.

2. Process chain for the production of therapeutic unique products

The existing process chain without considering the biomechanical simulation includes the image acquisition, the image post-processing and the rapid prototyping [4, 5]. The image raw data acquired using CT or MRI are segmented, visualized and transferred in a suitable data format by image post-processing. In the next step, a computer-aided design (CAD) model of the segmented objects is generated. Finally, these CAD data can be used to create a customized implant design [6]. This process chain can be expanded by biomechanical simulations to determine the patient-specific stress situation in spinal structures preoperatively. Based on this simulation, a patient-specific implant with an optimal fitting can be designed to reduce the risk of complications, incorrect loading conditions due to insufficient adapted implant design and adjacent segment degeneration. A possible expanded process chain could look like **Figure 1**, based on Hüsing et al. [1] and Rengier et al. [3].

The expanded process chain starts with the medical imaging or technical construction as the basis for the following three-dimensional (3D) reconstruction. After the three-dimensional reconstruction of the data, a biomechanical simulation model can be created. In a simulation model, morphological information and biomechanical properties of the patent-specific spine as well as of the corresponding implant are obtained. The aim of this biomechanical simulation is to ensure a "natural" stress distribution on the various spinal structures by the modeling of a patient-specific implant. Thus, overloading, which can lead to degenerative damage to the

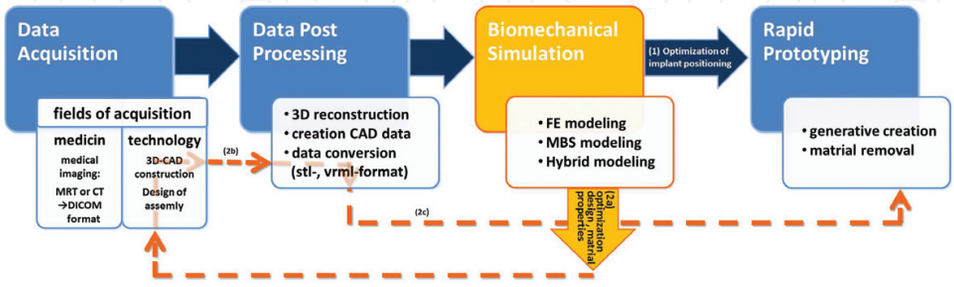

Figure 1. Expanded process chain with implemented biomechanical modeling.

head, should be avoided. This aim can be achieved by optimized positioning of the implant, an optimization of the implant design as well as of the implant material properties.

The goal of finding an optimal positioning (1) of an implant is in focus, which ensures, for example, a "natural" stress distribution, can be determined by the patient-specific simulation model. If desired, the exact coordinates of the positioned implant can be exported. These can then be taken into account in the operation planning. The rapid prototyping can be realized sequentially or in parallel.

If the baseplate design of a "standardized" implant is not suited to the morphological conditions of the contact surface of a patient-specific vertebral body, alternative baseplate designs can be demonstrated by means of a biomechanical simulation. In addition, corresponding modifications in implant material properties can also be analyzed and its effect on the spinal structures can be evaluated (see **Figure 1** process chain, loop (2a)). Thus, the risk of complications is minimized through, for example, an insufficient anchoring and the concomitant loosening of the implant or the occurrence of load peaks by point contact. On the basis of the simulation results, the implant can be re-designed specifically for a patient (see **Figure 1** process chain, loop (2b)), and corresponding input data (see **Figure 1** process chain, loop (2c)) can be generated for the further processing of rapid prototyping.

In the field of rapid prototyping, generative creations and processes with material removal can be different. Generative creation is the production of 3D physical models by applying material in thin layers and solidifying them. Established techniques are stereolithography, selective laser sintering, fused deposition modeling, laminated object manufacturing, and inkjet-printing techniques. A more detailed explanation can be taken from [3].

With such an expanded process chain, patient-specific implants can be produced not only with optimally shaped contact surfaces, which ensure a permanent fit of the implant without sinking and slipping, but also preoperative predictions can be made about the biomechanical effects of the implant and an optimized positioning can be proposed.

3. Medical imaging

Medical imaging is used as a basis for biomechanical modeling of the spine. Depending on the scientific question, these may be obtained from MRI cone beam computer tomography (CBCT), positron emission tomography (PET), single photon emission computed tomography (SPECT), and ultrasonography (US) [3]. From appropriate image data, using a specific image post-processing algorithm, 3D visualizations can be generated as well as an analysis of the biomechanical behavior of the tissue.

3.1. Segmentation and visualization

Since decades, the fully automatic segmentation of images—not only in the medical domain—is a challenge that is still unsolved in general [23, 35]. Not only the algorithms are the topic of research but also the question, how to evaluate the result of an image segmentation [33, 34].

Many modern segmentation algorithms in medical image processing use level sets; a review of these techniques can be found in [32]. State-of-the-art systems use the input of an expert to initialize segmentation and also allow for manual correction of the segmentation results.

To provide the input for modeling, the shape of the bones of a patient is required in three dimensions, which requires accurate segmentation. The key to success is to provide a computer assistance to speed up segmentation and to provide an interface that allows for fast and simple computer tools.

Bone structures are segmented in CT data. In those cases, where an MR image is also available, CT data and MR data are registered [36, 37] and fused. Most modern medical workstations provide such tools.

3.2. Defining biomechanical parameters

One possible way to determine the mechanical behavior of the spinal bony structures is to determine them from CT data. The radiation emitted during the scanning process penetrates the object and is weakened to varying degrees by the tissue. On the basis of the measured intensity reduction, an attenuation coefficient is calculated for each beam direction, to which a CT number is assigned. The unit of the CT number is given in Hounsfield [Hu] [6]. The Hounsfield unit is defined by the following equation:

$$H = 1000 * \frac{CT - CT_w}{CT_w - CT_a} \tag{1}$$

where CT_w and CT_a are the CT values of water and air [7]. According to Sun et al. [8], the CT number can be correlated to the density, for example, of the bone by a linear interpolation using relations available in published literature. The determined density can then be related to the so-called Young's modulus E. The heterogeneous elasticity, for example, of the cancellous and cortical bone, can in turn be defined by the following relationships [5]:

For cancellous bone, $CT < 816$:

$$\rho = 1.9 * 10E - 3 * CT + 0.105 \tag{2}$$

$$E = 0.06 + 0.9 * \rho * 2 \tag{3}$$

For cortical bone $CT > 816$:

$$\rho = 7.69 * 10 - E * 4 * CT + 1.028 \tag{4}$$

$$E = 0.09 + 0.9\rho 7.4 \tag{5}$$

In addition to determining biomechanical parameters by means of the CT number, it is also possible to obtain biomechanical information of, for example, the degree of intervertebral disc degeneration by a radiographic grading system. To determine more objective assessment of lumbar and cervical intervertebral disc degeneration, a new radiographic grading system [9, 10] is developed. The classification of this radiographic grading system is based on the three

variables "height loss," "steophyte formation," and "diffuse sclerosis." According to Wilke et al. [9], each of these three variables first has to be graded individually on lateral and postero-anterior radiographs. Finally, the so-called overall degree of degeneration is assigned on a four-point scale from 0 (no degeneration) to 3 (severe degeneration).

Recent approaches try to estimate biomechanical properties of humans by tracking motions both in color image sequences as in distance measurements. Such data are available from devices that were designed for consumer games, but have also been used experimentally in medical applications, for example, in Ref. [38].

4. Biomechanical modeling and simulation

Biomechanical modeling is an established method to simulate physics and physiology of a human body. Depending on the scientific question, it is possible to create whole body models for humans [11, 12] or parts of the body like the human heart [13, 14] or the spine [15, 16]. A distinction can be made between the multibody simulation (MBS) modeling and the finite element (FE) modeling. Depending on the scientific question, either the MBS or the FE simulation method can be used. For analyzing highly sophisticated problems, the FE modeling is the appropriate modeling method. The system is divided into a finite number of small geometric elements, called the finite elements. At the connection point, the so-called nodes, boundary and transition conditions are defined in accordance to specific material laws [17]. If the biomechanical behavior of high dynamic movements or larger parts or the entire of the human body is the focus, the MB simulation is the suitable method. A further possibility is to combine MBS and FE to ensure a higher degree of fine specific structure modeling. Due to such hybrid models (e.g. MBS-coupled with FE models), short computing times are guaranteed. The rapid availability of results enables a future usability in medical routine for spinal operation planning. Further detailed explanations of the basics of simulations can be taken out of [18].

4.1. Application examples implant design

The possibility of using the biomechanical simulation in the area of spinal surgery is diverse. Preoperatively, the effects of mono- or multisegmental spinal fusion on adjacent segments can be analyzed. In addition, an optimized positioning of the inserted implant can be demonstrated by taking into account the reconstruction of the sagittal balance or an adequate stress distribution. One can also compare the effects of minimally invasive surgical methods to surgical procedures with high degree of resections of spinal structures.

Although most manufacturers of implants offer different sizes of implants, a full-area contact of the implant with the vertebral body is not always ensured. An insufficient anchorage can lead to local stress peaks at the contact points. With the help of computer-assisted simulations, such stress peaks can be analyzed. To ensure the best possible anchoring, the effects of different contact surface designs of the implant can be determined. Thus, the simulation can contribute to a development of patient-specific shaped implant surfaces, which ensure a

permanent fit of the implant without sinking and slipping. Preoperatively, the effects of different implant lengths can also be analyzed.

The following simulations are intended as examples for a patient-specific problem and do not include the entire "expanded process chain," but only the subsection of the "biomechanical simulation." Thus, the following examples serve to illustrate the added value by the biomechanical modeling with regard to operation planning.

4.1.1. Effects of different standardized cage sizes

This example is intended to show the effects of the cage size on the biomechanics of the lumbar spine. For this, a biomechanical simulation a model of a person was created, which considers gender (male), age (35 years), weight (75 kg, body mass index (BMI) 22), and body height (1.85 m), including detailed lumbar spine structures (**Figure 2**). The lumbar spine model includes the biomechanical properties of the intervertebral discs, the facet joints, the ligamentous structures and the muscle groups left, right m. erector spinae, left and right m. rectus abdominus according to [21]. The exact model configuration as well as the validation can be found in Refs. [18–20].

To investigate the effects of fusing implants with five different sizes, the size of this optimally fitted implant is varied about ±2.5 and ±5%. In this context, an optimal fit is the planar resting of the cage on the endplates of the corresponding vertebral body. It should be noted that the entire cage base area is not in contact with the vertebral endplate, because it is a standardized implant without considering the patient-specific vertebral endplate morphology. The load situation, which is simulated, is the upright position under load of the body weight and a fused functional spinal unit (FSU) L4-L3. The weight force solves the kinematics of the MBS model and the motion equations, which form a system of coupled differential equations, are integrated for each simulation time step. This means that this weight force causes small movements in the spinal structures, and they are brought out of their equilibrium state. The reaction forces of the individual spinal structures build up until a new equilibrium state is reached. The following results refer to this new equilibrium state.

The basic implant size is chosen so that the implant fills the entire space between the corresponding vertebral bodies, and thus has contact with the endplates of the vertebral bodies. This basis cage is named in the **Figures 3–5** as "optimal fit." The cage is increased or reduced by a certain percentage and is shown in **Figures 3–5** as follows: "plus 2.5%" and "plus 5%" for the cages, which are enlarged 2.5 and 5%, respectively, and "minus 2.5%" and "minus 5%" for the size reduction of 2.5 and 5%, respectively (**Figure 3**).

When the basic cage is implemented in the FSU L3-L4, the other FSUs will undergo the least load compared to a smaller or larger cage size.

In the simulation cage "optimal fit," the lowest FSU sac-L5 is loaded the highest of all the FSU (**Figure 4**). The smallest stress is recorded in the FSU L5-L4. When a larger or smaller implant is selected, the load in all FSUs increases sharply. The load of the different FSUs hardly differ in height, whether the choice of a larger (plus 2.5% or plus 5%) or smaller (minus 2.5% or minus 5%) cage. The difference is marginal when comparing the simulations of the simulation cases "plus 2.5%," "plus 5%," "minus 2.5%," and "minus 5%" within the FSUs. The results show how

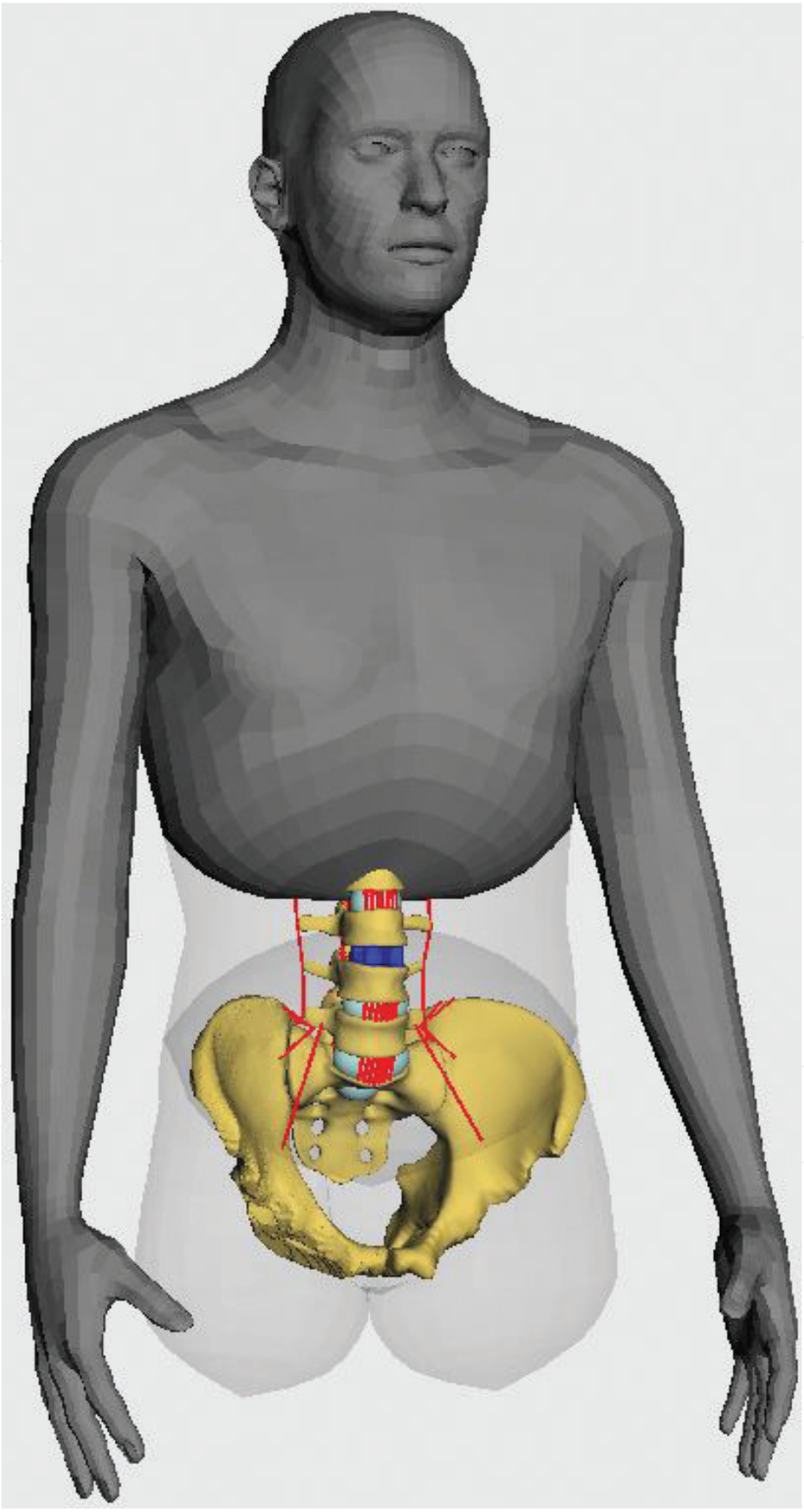

Figure 2. Simulation model of a person.

http://dx.doi.org/10.5772/intechopen.68835

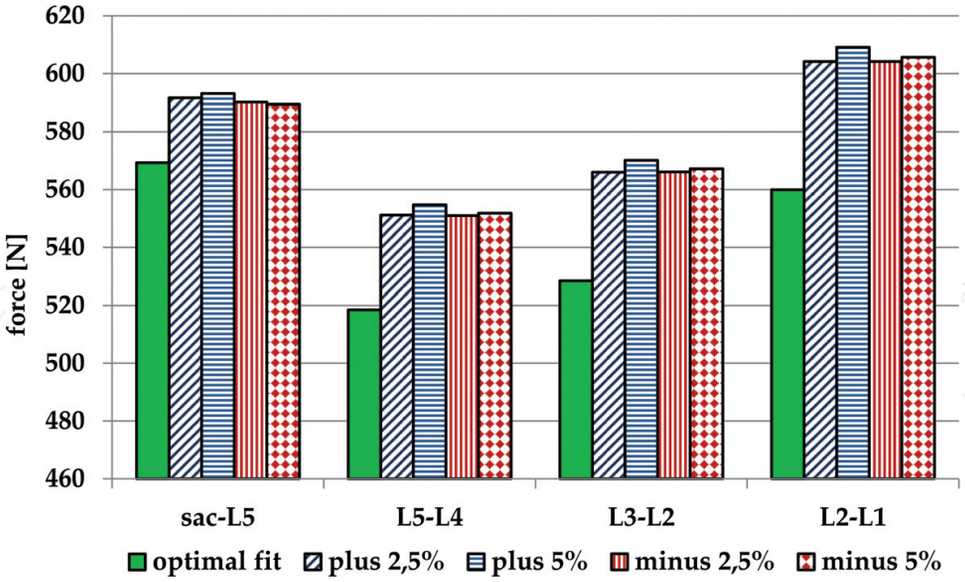

Figure 3. Vertical force intervertebral discs.

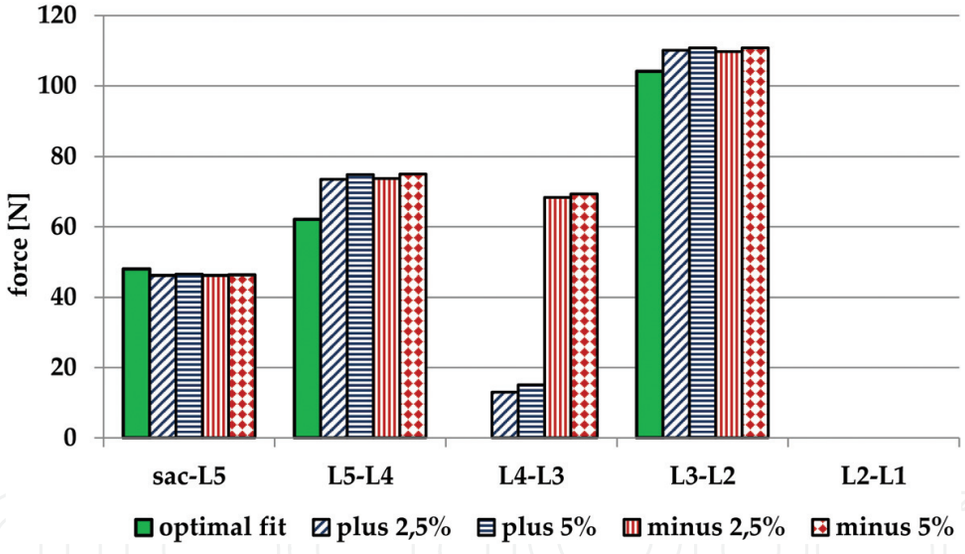

Figure 4. Loads of the facet joints.

important the correct choice of cage size could be, so that the intervertebral discs are not loaded more heavily.

On the other hand, if considering the loads of the facet joints, the choice of the implant size has a small influence on their load height. However, the facets of the FSU L3-L2 are much more heavily loaded than any other. This is due to the alignment of the facet surface. In the case of the FSUs L3-L2, the corresponding sagittal superior facet angles are relatively large so that the value of the force component of the acting external force, which is almost perpendicular to this surface, is high. Furthermore this FSU rotates in dorsal direction, so this boosts also the load situation. What's more, the facets joints of the FSU L4-L3 are not loaded in the cage when choosing the cage size "optimal fit." The reason is that the spinal alignment is modified by the body weight, so that

the vertebral bodies above the implemented cage FSU situated move in such a position that the lower endplate of FSU is in contact with the cage. As a result, the cranial facet joint surfaces of L4 and the caudal facet joint surfaces of L3 come directly and strongly into contact, and are therefore correspondingly highly loaded. The uppers facet joint L2-L1 are loaded in none of the simulation cases. The reason could be that the alignment of the facet joints is nearly parallel to the direction of movement, and so the facet surfaces "slide" through each other.

In general, the direction of rotation of the FSU is determined by the acting torque resulting from the lever arm and the acting weight force. Thereby, a force whose line of action runs vertically in front of the axis of rotation produces a positive torque, and a force whose line of action runs dorsally behind the axis of rotation produces a negative torque. A positive torque results in flexion movement, and a negative torque results in an extension movement of the affected vertebral body segments. From this model configuration or rather specific spinal alignment, the rotations seen in **Figure 5** are obtained. It should be noted, however, that these results are only valid for this model configuration and cannot be transferred to other patients. Already in the case of a changed spinal alignment, completely different results can occur [22]. But this example shows the effects of choosing a non-optimal fitting cage and the significance of the appropriate choice of the right cage size.

4.1.2. Cervical vertebral replacement

The superior surface of a cervical vertebral body is shaped like a tub. On its sides, it has small branches which are called uncinate processes. These margins build the uncovertebral joints (**Figure 6**) [23]. Thereby, the angle of the uncovered joints of the different vertebral bodies is not of the same magnitude, but increases significantly from C5 to C7 [24].

Due to the special anatomical conditions, the implantation of a vertebral body replacement implant or its baseplates cannot be optimally brought into contact with the corresponding superior or inferior anchor vertebra (**Figure 7**).

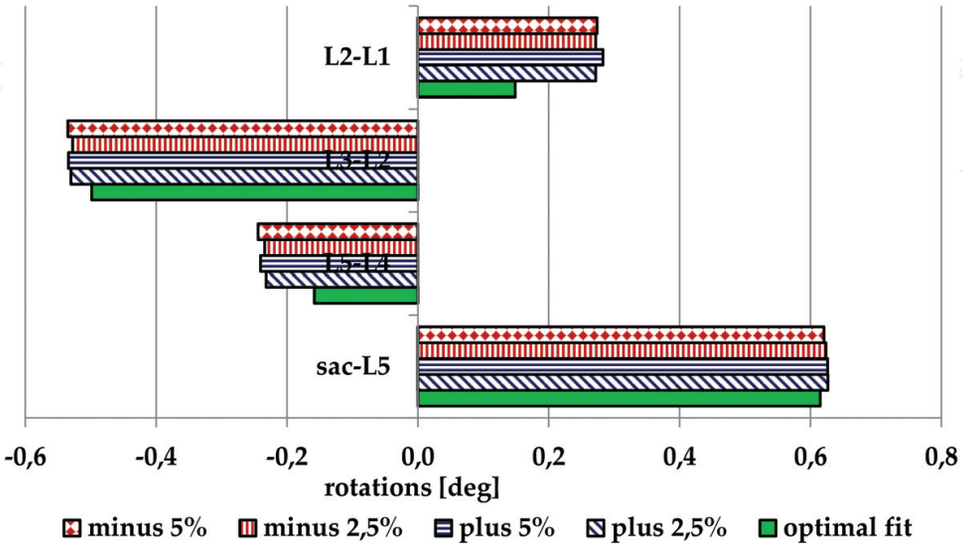

Figure 5. Rotation of the intervertebral discs.

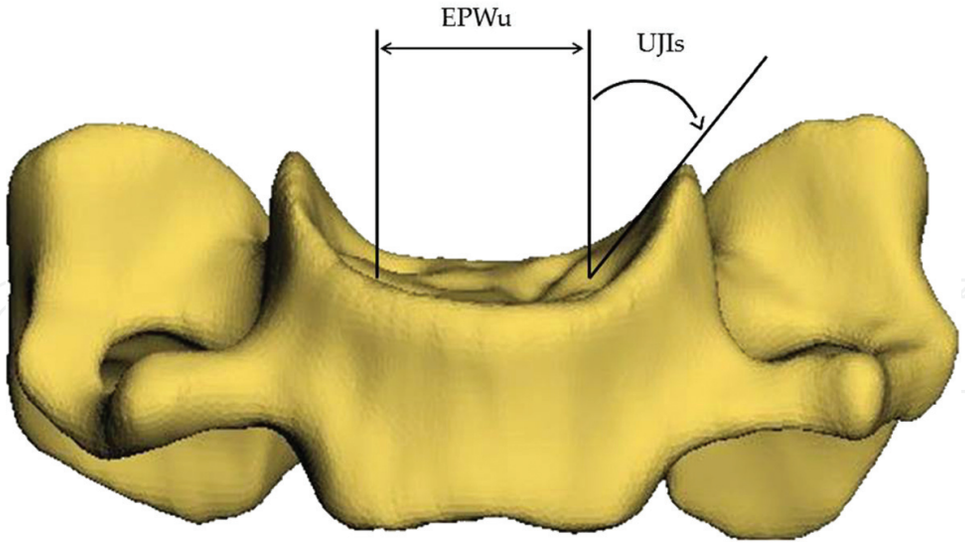

Figure 6. Illustration of the uncovertebral joint inclination.

In order to guarantee planar rest of the implant, the implant base should either be relatively narrow, so that it preferably rests only on the endplate surface of the corresponding vertebral body or be a "negative replica" of the patient-specific vertebral body surface, including consideration of the uncovered joint angle. A small implant baseplate has the disadvantage that the stress on the vertebral body is thereby increased by the reduced contact surface. A baseplate adapted to the superior vertebral surface could result in a much larger area of contact, and therefore a more balanced load distribution is achieved. Because this is a recently launched research project, the following examples are not intended to be final versions, but merely should represent the possibilities of a future implementation of biomechanical simulation in a process chain. The main focus will be to demonstrate the model creation and not to present validated results. The multibody simulation model is therefore a prototype. It should also be noted that we focus on the MBS modeling because this type of simulation is a much faster calculation method than the finite element method. In addition, we aim to implement fine-structured parts, such as the spine, into a whole-body model in order to simulate the dynamic situation of everyday life and thus to determine the stresses. Depending on the question, it is also possible to create a hybrid model of MBS and FE parts. A more detailed explanation can be found in Ref. [18] and in Section 5.

4.1.2.1. Basic model description

The MBS prototype model consists of the vertebral bodies C3-C6, where an extractable vertebral body replacement implant is implemented between the anchor vertebrae C3 and C6 (**Figure 8**). The intervertebral body surfaces C4 and C5 are adapted accordingly to the real operative procedure laminectomy. The anatomy of vertebral bodies C6 and C3 is retained. Because of the prevailing anatomical conditions of the uncovertebral joint and the relating lateral margins, a complete contact of the implant baseplates with the vertebral endplate of the anchor vertebra cannot be realized. As a result of the typically slightly corrugated form of the

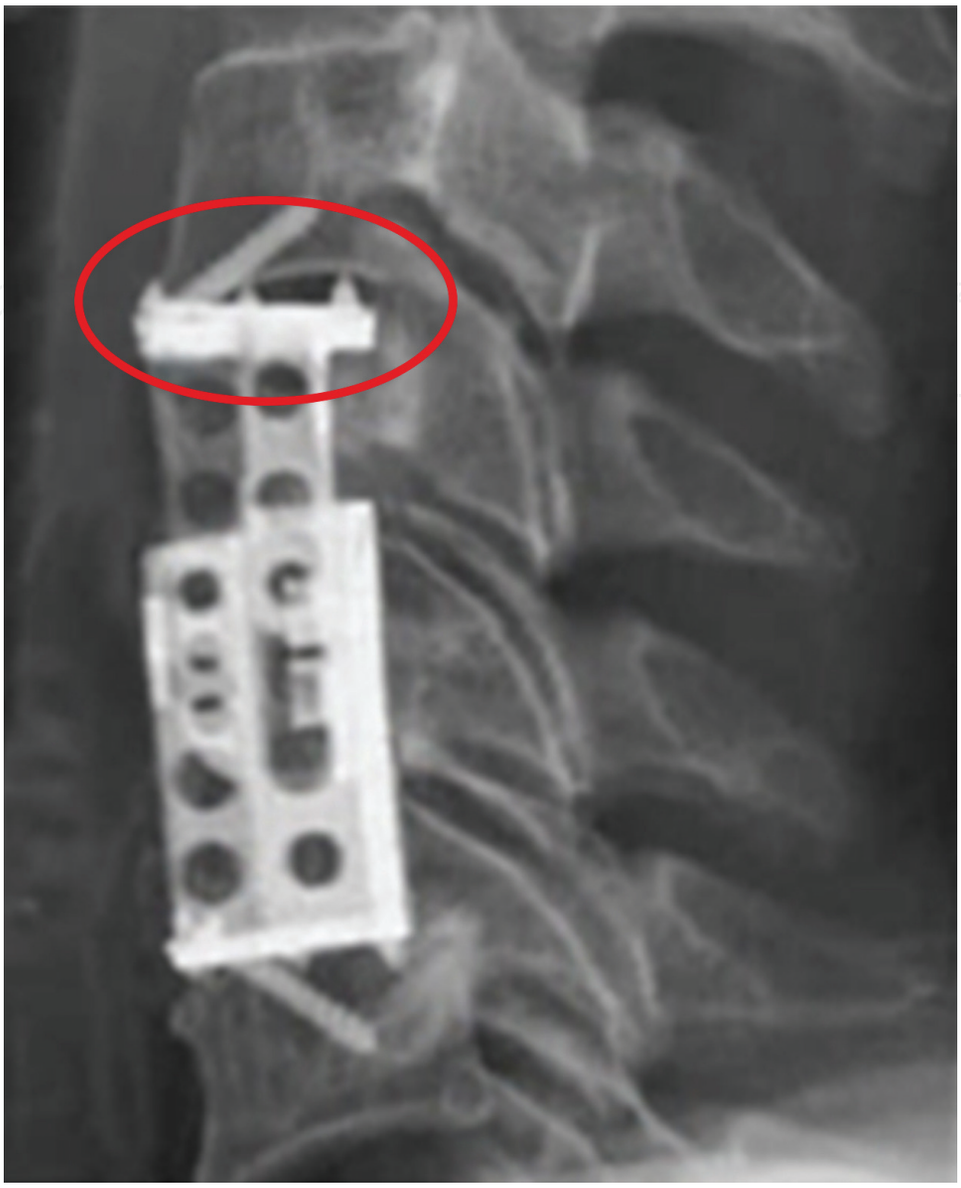

Figure 7. X-ray image of an implemented vertebral body replacement implant.

anchor vertebra, the parts of the implant base located medial have no direct contact with the anchor vertebra in the unload state. The cervical vertebral curvature corresponds to an average spine curvature and is 28 degrees [25]. The biomechanical properties of the ligaments and facet joints are taken from literature [26, 27].

4.1.2.2. Realization of the surface contact

The modeling of the contact between the vertebral body and the implant is realized by means of a special three-dimensional contact force element. The contacting surfaces, the baseplate of the implant, and the superior or inferior vertebral surface of the C3 and C6 are tessellated in such a way that the surfaces of the objects are composed of equally large polygons. In addition,

http://dx.doi.org/10.5772/intechopen.68835

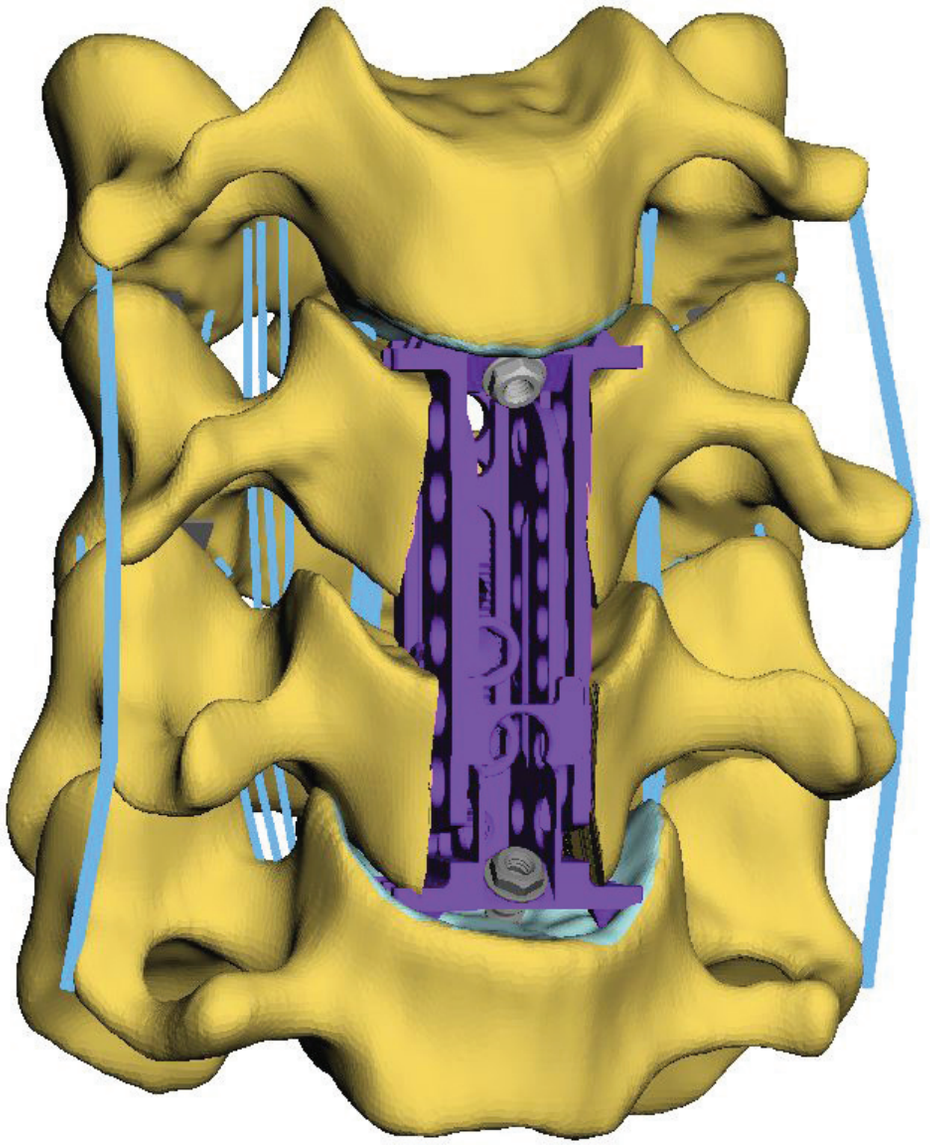

Figure 8. MBS model C6-C3 including vertebral body replacement implant.

the baseplate was dissected into smaller subunits to allow a more detailed analysis of the contact behavior (**Figure 9**).

For each of these polygons, a contact force is determined which is essentially oriented according to Hippmann [28] on the boundary layer model, and combined with a half-space approximation and contact force elements. So the contact force F_k is composed of a normal force F_{nk} and a tangential force F_{tk}. The normal force F_{nk} is composed as follows:

$$F_{nk} = \begin{cases} F_{ck} + F_{dk} : F_{ck} + F_{dk} > 0 \\ 0 : F_{ck} + F_{dk} \leq 0 \end{cases} \tag{6}$$

Annotation: in the following the subscript E and F stand for the corresponding bodies E and F. For the case $F_{ck} + F_{dk} > 0$, the equation is composed of a stiffness term,

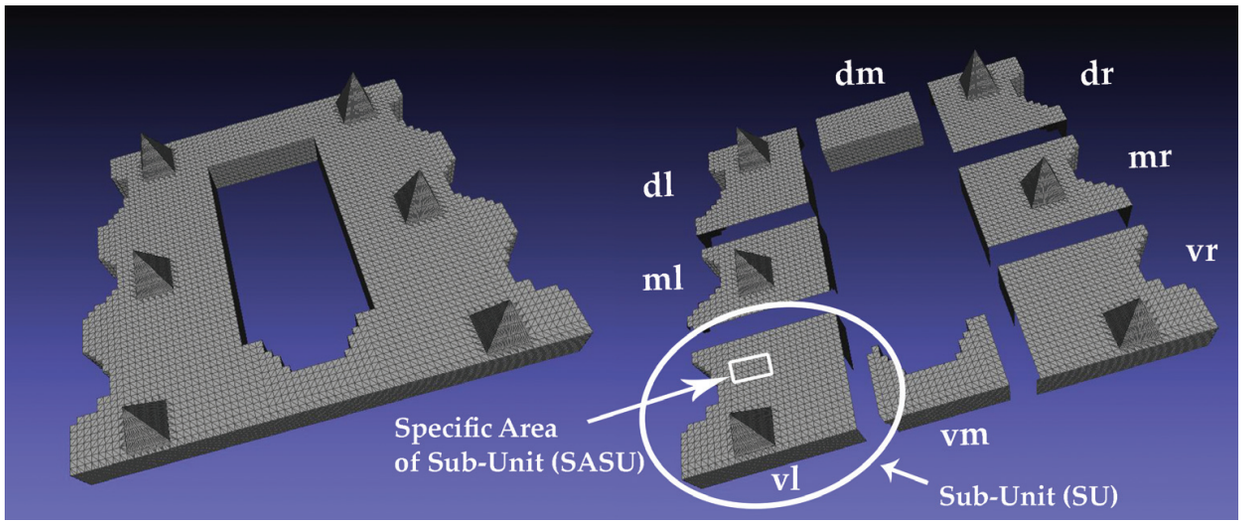

Figure 9. Illustration of the tessellated polygon meshes of the caudal implant base and explanation of terms.

$$F_{ck} = c_l * A_k * u_{nk} \tag{7}$$

c_l : stiffness of the contact element; A_k : total area of the contact element; u_{nk} : penetration of the contact element.

which results from

$$c_l = \frac{c_{lE} * c_{lF}}{c_{lE} + c_{lF}} \tag{8}$$

with

$$c_{lE} = \frac{K_E}{b_E} = \frac{1 - \nu_E}{(1 + \nu_E) + (1 - 2\nu_E)} * \frac{E_E}{b_E} \tag{9}$$

for c_{lF} analog and a damping term

$$F_{dk} = \begin{cases} d_l * A_k * v_{nk} : u_{nk} \geq u_d \\ d_l * A_k * v_{nk} * \dfrac{u_{nk}}{u_d} : u_{nk} < u_d \end{cases} \tag{10}$$

where

$$v_{nk} = n_k * v_k \tag{11}$$

stands for the relative speed projected in the normal direction

$$v_k = v_{M_e M_f} + \omega_{M_e M_f} \times r_{M_f C_k} \tag{12}$$

of both contact bodies at the position c_k of the contact element.

http://dx.doi.org/10.5772/intechopen.68835

According to Hippmann [28], the parameter u_d can be used to define a penetration depth up to which the damping force acts linear. This makes it possible to avoid unrealistic forces during rapid contact processes. Further input parameters are the layer depth b, the E-modulus, and Poisson's ratio ν of each surface and the damping constant d. Because the vertebral body replacement implant consists of a titanium alloy, the corresponding material property for E and ν has been entered into the model. The E-modulus and Poisson's ratio ν for the superior and inferior vertebral body surfaces are taken from [29, 30]. The damping is 10% of the E-modulus of the vertebral body replacement implant. The resulting total force of the contact surface is determined by summing the acting forces of all contact elements. Because the vertebral body replacement implant is actually fastened to the vertebral body by means of a screw, this fixation has been realized by a force element that realizes spring and damper forces and moments between bodies in multiple axis direction. These parameters ($c = 108$ N/m, $d = c * 0.1$ Ns/m) are determined by means of sensitivity analysis.

The tangential force F_{tk} is calculated as follows [28] and is determined in dependence of the tangential relative velocity

$$v_{tk} = v_k - v_{nk} * n_k \tag{13}$$

$$v_{tk} = |v_{tk}| \tag{14}$$

and the normal force F_{nk} of the contact element

$$F_{tk} = \begin{cases} \mu * F_{nk} : \ v_{tk} \geq v_\varepsilon \\ \mu * F_{nk} * \dfrac{v_{tk}}{v_\varepsilon} * \left(2 - \dfrac{v_{tk}}{v_\varepsilon}\right) : \ v_{tk} < v_\varepsilon \end{cases} \tag{15}$$

To avoid a set-valued static friction, the frictional force is disabled when the sliding speed falls below a given small value v_ε.

The total force F_k and the torque M_k of the single contact element are now:

$$F_k = F_{nk} * n_k + F_{tk} * \frac{\mathrm{v}_{tk}}{v_{tk}} \tag{16}$$

$$M_k = r_{M_f C_k} \times F_k \tag{17}$$

Finally, the forces and torques of all contact elements are summed to the resulting total force screw:

$$F_E^{M_f} = \sum\nolimits_k F_k \tag{18}$$

$$M_E = \sum\nolimits_k M_k \tag{19}$$

A detailed description of the determination of the contact force and further information can be found in [28].

4.1.2.3. Simulation results

The external force that causes the kinematics of the model is 50 N, which corresponds to the average weight force of the corresponding upper body segments and is taken from [31]. In general, it is possible to analyze both the kinematic and kinetic parameters of the modeled spinal structures in this model configuration, such as the ligaments or facet joints, as well as the contact behavior "vertebral body surface-implant plate." In the following, the contact behavior is analyzed and the parameters "total contact patch area," "weighted penetration," "maximum penetration," "maximum contact pressure," and "weighted contact pressure" are discussed.

The surfaces of the subunits of the caudal implant base surface, which comes into contact with the superior anchor vertebral surface, are of different size (**Table 1**). The sinister regions are more in contact than the dexter regions.

Both the dorsally central (dm) and dorsally dexterous region (dr) of the implant baseplate have no contact with the vertebral body C6. The percentage total contact surface is 52%.

The average penetrations and the maximum penetrations of the subunits are shown in **Figure 10**. The right front (vr) and central front (vm) subunits penetrate the superior vertebral body surfaces on average most strongly. The weighted penetration of the left middle (ml) and right middle (mr) subunits is half as high. Due to the missing contact in the subunits "dm"and "dr," there is no penetration.

The maximum penetration behaves in an analogous manner. The difference between the "weighted penetration" and the "maximum penetration" of the ventral right "vr" and the left dorsal "ld" subunit stands out. The maximum penetration is 2.5 times and 2 times higher than the weighted penetration. In the remaining subunits, the maximum penetration is more than 1.5 times higher than the weighted penetration. We concluded that within the different subunits (SU) the penetration depth of the specific areas of this subunit (SASU) can be very different in some cases.

	Percentage contact patch area (%)
vr	15.0
vm	9.8
vl	1.3
ml	15.7
dl	1.2
dm	0.0
dr	0.0
mr	8.9

Table 1. Percentage contact of the subunits of the implant base with the vertebral endplate.

http://dx.doi.org/10.5772/intechopen.68835

Looking at the contact pressure in **Figure 11**, the right ventral (rv) subunit of the implant baseplate is much more heavily loaded than the other subunits. The maximum contact pressure in this subunit of the implant base is 6 times stronger and the weighted contact pressure is 5 times stronger. Comparing the maximum and the weighted contact pressure of the right ventral (rv) subunit, the subunit "rv" certain specific areas of subunit are loaded up to 2.5 times more than others.

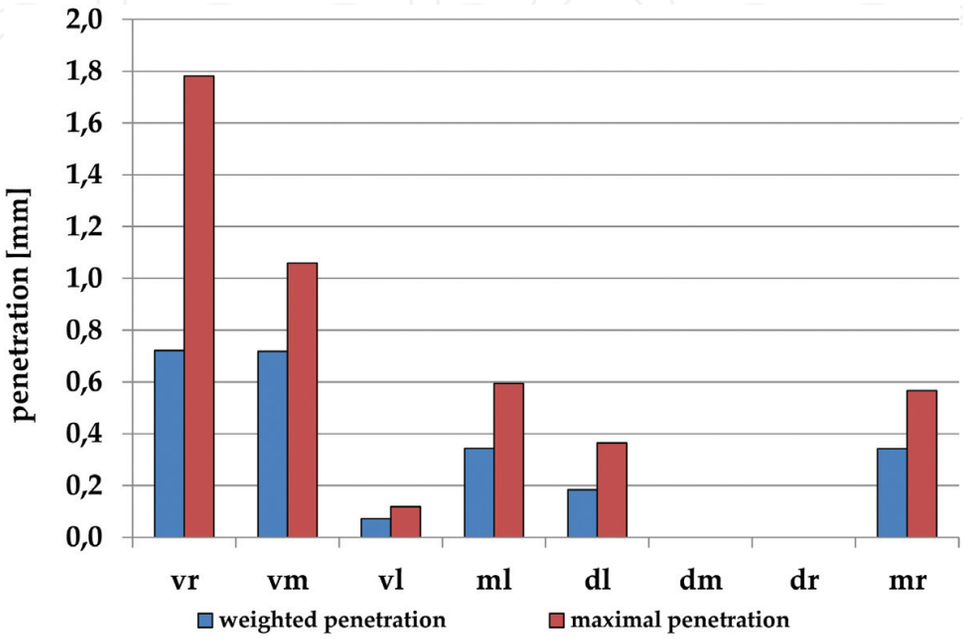

Figure 10. Penetration of the contact surfaces.

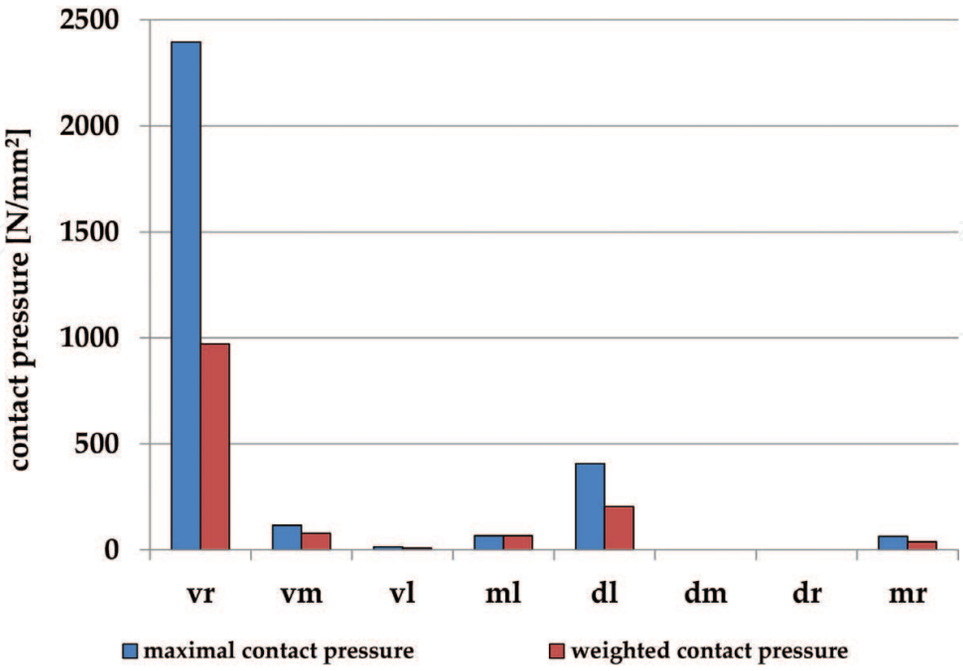

Figure 11. Contact pressure of the different subunits.

5. Summary and discussion

In many fields, personalized medicine has already been successfully introduced. In spinal implant surgery, patient-specific implants with an optimized fit shape could minimize severe complications. Depending on the question of cause, it is also possible to disassemble the basis plate of the implant into even smaller subunits in order to be able to make more detailed statements. If necessary, a hybrid model consisting of MBS and FE parts can also be created. However, it is always important to consider how exact the model must be. The desired precision determines how many more parameters, whose biomechanical properties must be known, flow into the model. However, some of these biomechanical parameters can only be inadequately determined. Furthermore, the calculation time increases with the increase in the fine structure of the model.

The presented modeling should not be seen as a competition to the FE modeling because our aim is to pursue a holistic way of looking at patients. Therefore, detailed models should be implemented in a whole-body model to simulate dynamic everyday situations and to obtain patient-specific knowledge about the stress situation in the fine-structured area. A valid modeling is indispensable, which can be ensured by selecting suitable input parameters. Because personalized input parameters of the model are often difficult to determine, we try to develop a procedure for the determination of patient-specific biomechanical properties of the human structures, which also guarantees rapid availability of these data as input parameters for the modeling.

Author details

Bauer Sabine[1]* and Paulus Dietrich[2]

*Address all correspondence to: bauer@uni-koblenz.de

1 Institute for Medical Engineering and Information Processing, University Koblenz-Landau, Koblenz, Germany

2 Institute for Computer Science, University Koblenz-Landau, Koblenz, Germany

References

[1] Hüsing B, Hartig J, Bührlen B, Reiß T, Gaisser S. Individualisierte Medizin und Gesundheitssystem. Future Report. 2008;126:1–348 Available from: http://www.tab-beim-bundestag.de/de/pdf/publikationen/tab-brief/TAB-Brief-034.pdf

[2] FDA USA Food and Drug Administration. Paving the Way for Personalized Medicine: FDA's Role in a New Era of Medical Product Development. 1st ed. U.S. Department of Health and Human Services; 2013; Silver Spring, USA. p. 62. DOI: http://www.fda.gov/downloads/…/PersonalizedMedicine/UCM372421….

[3] Rengier E, Mehndiratta A, von Tengg-Kobligk H, Zechmann C, Unterhinninghofen R, Kauczor H.-U, Giesel F. 3D printing based on imaging data: Review of medical applications. International Journal of Computer Assisted Radiology and Surgery. 2010;**5**(3):335-341. DOI: 10.1007/s11548-010-0476-x 2010

[4] Sauer A, Beneke F, Bergers D, Witt G. Modelle und Prototypen für die Medizin. RTejournal. 2005;**2**(2):1-10. Available from: http://. www.rtejournal.de/ausgabe2/69

[5] Ay M, Kubat T, Delilbasi C, Ekici B, Yuzbasioglue H, Hartomacioglub S. 3D Bio-Cad modeling of human mandible and fabrication by rapid-prototyping technology. Usak University Journal of Material Sciences. 2013;**2**:135-145. DOI: 10.12748/uujms.201324255

[6] Kauffmann G, Sauer R, Weber W. Radiologie: Bildgebende Verfahren, Strahlentherapie, Nuklearmedizin und Strahlenschutz. 4th ed. München, Jena: Urban & Fischer Verlag/Elsevier GmbH; 2011. p. 320

[7] Rho J, Hobantho M, Ashman R. Relations of mechanical properties to density and CT numbers in humanbone. Medical Engineering and Physics. 1995;**17**(5):347

[8] Sun W, Starly B, Nam J, Darling A. Bio-CAD modeling and its applications in computer-aided tissue engineering. Computer-Aided Design. 2005;**37**:1097-1114

[9] Wilke H-J, Rohlmann F, Neidlinger-Wilke C, Werner K, Claes L, Kettler A. Validity and interobserver agreement of a new radiographic grading system for intervertebral disc degeneration: Part I. Lumbar spine. European Spine Journal. 2006;**15**(6):720-730. DOI: 10.1007/s00586-005-1029-9

[10] Kettler A, Rohlmann F, Neidlinger-Wilke C, Werner K, Claes L, Wilke, H-J. Validity and interobserver agreement of a new radiographic grading system for intervertebral disc degeneration: Part II. Cervical spine. European Spine Journal. 2006;**15**(6):732-741. DOI: 10.1007/s00586-005-1037-9

[11] Rajagopal A, Dembia C, DeMersm M, Delp D, Hicks J, Delp S. Full-body musculoskeletal model for muscle-driven simulation of human gait. IEEE Transactions on Biomedical Engineering. 2016;**63**(10):2068-2079 DOI: 10.1109/TBME.2016.2586891

[12] Östh J, Brolin K, Bråse D. A human body model with active muscles for simulation of pretensioned restraints in autonomous braking interventions. Traffic Injury Prevention. 2014;**16**:304-313. DOI: 10.1080/15389588.2014.931949

[13] Stapleton S, Moreira R, Jockenhoevel S, Mela P, Reese S. Effect of reinforcement volume fraction and orientation on a hybrid tissue engineered aortic heart valve with a tubular leaflet design. Advanced Modeling and Simulation in Engineering Sciences. 2015;**2**(21):1-17. DOI: 10.1186/s40323-015-0039-3

[14] Baillargeon B, Rebelo N, Fox D, Taylor R, Kuhl E. The living heart project: A robust and integrative simulator for human heart function. European Journal of Mechanics A/Solids. 2014;**48**:38-47. DOI: 10.1016/j.euromechsol.2014.04.001

[15] Ignasiak D, Sperr R, Ferguson S. The effect of age-related changes in spinal kinematics on vertebral loading during daily living activities. In: 22nd Congress of the European Society

of Biomechanics; July 10-13, 2016; Lyon, France. 2016. DOI: https://esbiomech.org/conference/index.php/congress/lyon2016/paper/view/188

[16] Schmidt H, Heuer F, Wilke H-J. Interaction between finite helical axes and facet joint forces under combined loading. Spine. 2008;**33**(25):2741-2748. DOI: 10.1097/BRS.0b013e31817c4319

[17] Schwertassek R, Wallrapp O. Dynamics of flexible multibody systems. Methods of mechanics for computer-aided design and analysis of mechatronic systems. Wiesbaden: Vieweg+Teubner Verlag; 1999. p. 476 DOI: 10.1007/978-3-322-93975-3

[18] Bauer S. Basics of multibody systems: Presented by practical simulation examples of spine models. In: Lopez-Ruiz R, editor. Numerical Simulation—From Brain Imaging to Turbulent Flows. Rijeka, Croatia: Intech; 2016. pp. 29-49. DOI: 10.5772/62864

[19] Bauer S, Paulus D. Analysis of the biomechanical effects of spinal fusion to adjacent vertebral. International Journal of Simulation-Systems, Science and Technology—IJSSST. 2015;**15**(2):1-7. DOI: 10.1109/EMS.2013.28

[20] Bauer S, Keller E, Paulus D. Rückenschmerz durch Übergewicht? Biomechanische MKS-Modellierung der Belastungssituation der Lendenwirbelsäule bei unterschiedlichem Körpergewicht. In: Handels Heinz, Thomas Martin D, Hans-Peter M, Thomas T, editors. Bildverarbeitung für die Medizin 2015; 15. bis 17. März 2015 ; Lübeck. Berlin, Heidelberg: Springer; 2015. pp. 323-328. DOI: 10.1007/978-3-662-46224-9

[21] Rohlmann A, Bauer L, Zander T, Bergmann G, Wilke H-J. Determination of trunk muscle forces for flexion and extension by using a validated finite element model of the lumbar spine and measured in vivo data. Journal of Biomechanics. 2006;**39**(6):981-989

[22] Juchem S, Hausen U, Gruber K. Effects on individual spine curvatures—A comparative study with the help of computer modelling. In: Olaf D, editor. Biomedical Engineering; 16.09.2016–19.09.2016; Jena, Germany. De Gruyter; 2012. pp. 132-135. DOI: https://doi.org/10.1515/bmt-2012-4052

[23] Tubbs R, Rompala O, Verma K, Mortazavi M, Benninger, B, Loukas, M, Chambers R: Analysis of the uncinate processes of the cervical spine: An anatomical study. Journal of Neurosurgery: Spine. 2012;**16**:401-407. DOI: 10.3171/2011.12.SPINE11541

[24] Panjabi M, Duranceau J, Goel V, Oxland T, Takata K. Cervical human vertebrae—quantitative three-dimensional anatomy of the middle and lower regions. Spine. 1991;**16**(8):861-869. DOI: 10.1007/s00586-003-0586-z

[25] Grob D, Frauenfelder H, Mannion H. The association between cervical spine curvature and neck pain. European Spine Journal. 2007;**16**:669-678. DOI: 10.1007/s00586-006-0254-1

[26] Yoganandan N, Kumaresan S, Pintar FA. Biomechanics of the cervical spine Part 2. Cervical spine soft tissue responses and biomechanical modeling. Clinical Biomechanics. 2001;**16**:1-27. DOI: http://dx.doi.org/10.1016/S0268-0033(00)00074-7

[27] White A, Panjabi M. Clinical Biomechanics of the Spine. University of Michigan: Lippincott; 1978. p. 534

[28] Hippmann G. Modellierung von Kontakten komplex geformter Körper in der Mehrkörperdynamik [dissertation]. Wien: TU Wien; 2004. p. 175. Available from: http://elib.dlr.de/12219/

[29] Kurutz M. Finite element modeling of the human lumbar spine. In: Moratal D, editor. Finite Element Analysis. Rijeka, Croatia: InTech; 2010. pp. 209-236. DOI: http://www.intechopen.com/books/finiteelement-

[30] Kumaresan S, Yoganandan N, Pintar F, Maiman D. Finite element modeling of the cervical spine: Role of intervertebral disc under axial and eccentric loads. Medical Engineering & Physics. 1999;**21**:689-700

[31] Panjabi M, Summers D, Pelker R, Videman T, Friedlaender G, Southwick W. Three-dimensional load-displacement curves due to forces on the cervical spine. Journal of Orthopaedic Research. 1986;**4**:152-161. DOI: 10.1002/jor.1100040203

[32] Cremers D, Rousson M, Deriche R. A review of statistical approaches to level set segmentation: Integrating color, texture, motion and shape. International Journal of Computer Vision. 2007;**72**:195-215. doi:10.1007/s11263-006-8711-1

[33] Zhang YJ. A survey on evaluation methods for image segmentation. Pattern Recognition. 1996;**29**(8):1335-1346. DOI: 10.1016/0031-3203(95)00169-7

[34] Fenster A, Chiu B. Evaluation of segmentation algorithms for medical imaging. In: Proceedings of Annual International Conference of the IEEE Engineering in Medicine and Biology Society. IEEE Engineering in Medicine and Biology Society Conference; 2005. DOI: 10.1109/IEMBS.2005.1616166

[35] Zhu H, Meng F, Cai J, Lu S. Beyond pixels. A comprehensive survey from bottom-up to semantic image segmentation and cosegmentation. Journal of Visual Communication and Image Representation. 2016;**34**:12-27

[36] Fitzpatrick J, Hill D, Maurer C. Image Registration. Handbook of Medical Imaging. Medical Image Processing and Analysis. 2000;**2**:447-514

[37] Wyawahare MV, Patil PM, Abhyankar HK. Image registration techniques: An overview. International Journal of Signal Processing, Image Processing and Pattern Recognition. 2009;**2**(3):11-28

[38] Junyi X, Alfredo S. A real-time respiratory motion monitoring system using KINECT: Proof of concept. Journal of Medical Physics. 2012;**39**(5):2682-2685. doi:10.1118/1.4704644

IntechOpen